Deformation Microstructure and Recovery

Yu, Tianbo

Published in:
Recrystallization

Publication date:
2020

Document Version
Peer reviewed version

Chapter

DEFORMATION MICROSTRUCTURE AND RECOVERY

Tianbo Yu*

Department of Mechanical Enigneering, Technical University of Denmark, Kgs. Lyngby, Denmark

ABSTRACT

This chapter is devoted to the topics of deformation microstructure and recovery. The conventional notations and understandings of recovery at low strains are briefly reviewed, followed by a presentation of materials and processing parameters controlling recovery and the microstructure-property relationship during recovery. New discoveries on deformation microstructures from the last 30 years are briefly reviewed with focus on face-centered cubic (FCC) metals with high stacking fault energy. The strong effect of microstructure on recovery is exemplified by a presentation of novel dynamic and static recovery mechanisms in ultrafine microstructures.

Deformation microstructure not only determines the properties of a deformed metal but also provides the driving force for recovery and recrystallization; recovery competes with recrystallization in restoring microstructure and properties and at the same time facilitates nucleation of recrystallization. Therefore, such topics are important in the design, processing and understanding of novel metals with optimized properties.

Keywords: deformation microstructure; dynamic/static recovery; dislocation; geometrically necessary boundary (GNB); incidental dislocation boundary (IDB); triple junction migration

*Corresponding Author Email: tiyu@mek.dtu.dk

1. INTRODUCTION

Metallic components are typically produced by thermomechanical processing where plastic strain and temperature are key parameters. The processing brings the metal towards an appropriate shape, produces heat, and changes the microstructure of the metal. The deformed microstructure stores a small fraction of the total deformation energy in the form of lattice defects, which greatly alter the mechanical and physical properties of the metal. In the deformed state, the metal has a high stored energy thus a driving force for the deformation microstructure to return to its undeformed soft state.

Recovery is the first restoration process taking place in a deformed microstructure. In a collective review (Doherty et al. 1997), it was defined as "all annealing processes occurring in deformed materials that occur without the migration of a high angle grain boundary", whose misorientation angle is typically larger than 15°. Recovery is a precursor of recrystallization, which is the formation of a new grain structure in a deformed material by the formation and migration of high angle grain boundaries driven by the stored energy in the microstructure. Recovery includes many processes; depending on the materials and processing parameters, such processes may also occur during plastic deformation as dynamic recovery. Dynamic recovery plays an important role during plastic deformation and, together with deformation mechanisms, determines the deformation microstructure.

The extensive early work on deformation microstructure and recovery has been reviewed previously by a number of authors (Beck 1954; Bever 1957; Perryman 1957; Friedel 1964; Li 1966; Bever, Holt, and Titchener 1973; Gil Sevillano, van Houtte, and Aernoudt 1980; Nes 1995). Recent reviews can be found in (Niels Hansen and Barlow 2014; Raabe 2014; Humphreys, Rollett, and Rohrer 2017) and the proceedings of the 36th Risø International Symposium on Materials Science (Fæster et al. 2015). The present work starts with a review of old notations and descriptions of recovery (mainly at low strain), and then focuses on new discoveries in deformation microstructures and recovery mechanisms found in heavily deformed metals.

2. RECOVERY OF DISLOCATION STRUCTURES AT LOW STRAINS

2.1. Dislocation accumulation

Plastic deformation of metals takes place predominantly by glide of dislocations on the slip plane, causing the macroscopic strain (Friedel 1964; Hull and Bacon 2001). The stress required to deform the metal increases with increasing strain—the metal work hardened (strain hardened). This is because many generated dislocations are stored in the structure thus become immobile. Plastic deformation is therefore accompanied by an increase in the density of dislocations, which resist further dislocation glide. Annealed metals typically contains a dislocation density of 10^8 - 10^{10} m/m^3, and this parameter can increase to about 10^{13} - 10^{14} after 10% deformation and continues to increase as the strain increases further. The dislocations represent an energy per unit length; the stored energy of the deformed material is proportional to the dislocation density.

Different from slip by dislocation glide, twinning is a characteristic deformation mechanism for face-centered cubic (FCC) metals of low stacking fault energy and hexagonal close-packed (HCP) metals. However, twinning is less common than slip and twin boundaries are stable during recovery. Plastic deformation also produces point defects, i.e. vacancies and interstitials, but most of the point defects typically anneal out quickly after deformation unless the sample is deformed and subsequently stored at a very low temperature. Therefore, we shall in this section only discuss phenomena related to the dislocation structures introduced by plastic deformation.

2.2. Dislocation annihilation

During recovery, dislocation rearrangement occurs by glide, climb and cross slip of dislocations, reducing the stored energy in the metal as a result of dislocation annihilation. A number of annihilation processes have been analyzed in the literature (Friedel 1964; Li 1966) and they depend on many parameters, such as the material, strain level, strain rate, deformation temperature, and annealing temperature and time. Annihilation of dislocations may occur in a number of ways during annealing:

- Dislocations can glide to the sample surface as can be seen from slip steps;

- Dislocations can interact with a high angle grain boundary and get absorbed;
- Dislocation pairs with opposite Burgers vectors can annihilate by glide, assisted by climb (edge dislocation) and cross slip (screw dislocation) if they are not on the same slip plane.

These processes reduce the dislocation density in the deformed metal. For simple dislocation arrays, the kinetics of dislocation recovery was analyzed in detail by Li (Li 1966). For a complex dislocation structure, the recovery kinetics is typically found to be close to logarithmic, and it has been expressed as (Borelius, Berglund, and Sjoberg 1952):

$$\frac{dP}{dt} = -K_0 P \exp(-\frac{Q_0 - \beta P}{RT}) \tag{1}$$

where P is the stored energy (proportional to the dislocation density), t is the annealing time, T is the annealing temperature, R is the gas constant, Q_0 is the activation energy at the end of recovery, and the three fitting parameters K_0, Q_0 and β are associated with the active recovery mechanisms. Similar but slightly different forms have also been suggested initially by Kuhlmann-Wilsdorf (Kuhlmann 1948). Important in these models is that the apparent activation energy (Q_0-βP) increases as recovery proceeds (Kuhlmann 1948; Cottrell and Aytekin 1950; Borelius, Berglund, and Sjoberg 1952; Michalak and Paxton 1961; Friedel 1964; Nes 1995; Rath and Pande 2013). The increase of the activation energy is related to the decrease of the stored energy (driving force) during recovery, making it more difficult for recovery to proceed.

2.3. Dislocation rearrangement

There are a large fraction of dislocations in the deformed microstructure that are difficult to annihilate by the above mechanisms. During recovery, these excess dislocations have a tendency to form low energy configurations such as dislocation walls and low angle boundaries, accommodating the lattice curvature imposed by the strain. In these configurations, the dislocations mutually compensate their distortion fields and thus reduce the total elastic energy. For a low angle boundary, it is described by the Read–Shockley equation (Read and Shockley 1950) that the total energy γ increases but the energy per unit dislocation length decreases with increasing density of dislocations in the boundary, i.e. with increasing boundary misorientation angle θ:

$$\gamma(\theta) = \begin{cases} \gamma_m \dfrac{\theta}{\theta_m}\left[1 - \ln\left(\dfrac{\theta}{\theta_m}\right)\right], \theta \le \theta_m \\ \gamma_m \qquad\qquad\qquad\qquad , \theta > \theta_m \end{cases} \tag{2}$$

where γ_m is the energy per unit area of a high angle boundary and θ_m is usually taken as 15°. These excess dislocations therefore tend to form fewer boundaries of higher misorientation angles, i.e. reducing their total energy.

A simple case of forming a low angle boundary is termed glide polygonization, which was first demonstrated by Cahn (Cahn 1949), who bent and annealed a single crystal and observed that excess dislocations of one kind distributed on the slip plane will rearrange into low angle boundaries perpendicular to the slip planes upon annealing, thereby reducing the total stored energy.

In the general case of deformation of polycrystalline materials, dislocations of different Burgers vectors are generated and some of them remained in the structure. During annealing, these dislocations react and arrange into three-dimensional (3D) structures, where a classic example is a cell structure with a high dislocation density in the cell walls and a low dislocation density in the cell interior. With further annealing, recovery proceeds both in the cell walls and in the cell interior. Cell walls become sharper and sharper by removing dislocation pairs of opposite Burgers vectors through mutual annihilation and rearranging the excess dislocations into low angle boundaries. Such a structure with sharp low angle boundaries and almost dislocation free interior is called a subgrain structure.

2.4. Dynamic Recovery

The rearrangement and annihilation of dislocations occur not only during annealing but also in the course of deformation as dynamic recovery. Dynamic recovery is partially thermally activated and stress/strain assisted. It reduces both the energy storage rate and the work hardening rate. For metals of high stacking fault energy, dynamic recovery occurs readily during deformation, forming 3D cell/subgrain structures in the deformed samples (Figure 1).

The organization of the dislocation structure in a deformed sample may be considered as a result of dynamic recovery. Alternatively, this configuration may be interpreted based on the low energy dislocation structure (LEDS) hypothesis (Kuhlmann-Wilsdorf 1989) that dislocations arrange to reduce the energy per unit length of dislocation line. The ability of dislocations to reach their lowest-energy configurations is constrained by a number of factors, including the number of

available slip systems, the dislocation mobility (for both glide and climb), and the frictional stress.

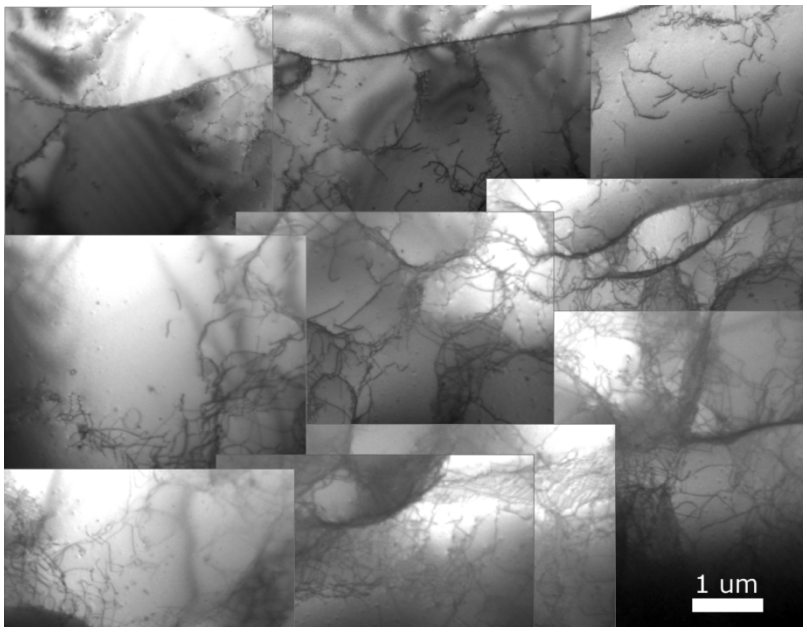

Figure 1. Montage of a cell structure (in a grain of Cube texture) in the longitudinal section of Al (99.996% purity) after 10% cold rolling.

2.5. Subgrain growth

The initial size of cells/subgrains depends on the materials and processing parameters, and is in the order of 1 μm. The energy stored in these cell/subgrain boundaries are the driving force for subgrain growth, which reduces the stored energy by reducing the boundary area. The growth of subgrains is typically continuous (uniform coarsening, normal subgrain growth) but it can also be discontinuous (non-uniform coarsening, abnormal subgrain growth). Figure 2 shows an example of a subgrain structure in annealed Al with very few dislocations inside subgrains.

Migration of subgrain boundaries (Smith and Dillamore 1970; Sandstrom 1977; Nes 1995; Humphreys, Rollett, and Rohrer 2017) is considered as the dominant mechanism for subgrain growth. The mobility of low angle subgrain boundaries is generally lower than that of high angle boundaries, and increases with increasing misorientation angle. However, dislocation boundaries with very

low misorientation angles (e.g. below 1°) may have a high mobility, especially under the influence of local residual stresses. Moreover, such boundaries may disappear by continuously reducing their misorientation angle through rotation and coalescence – an alternative mechanism of subgrain growth (Jones, Ralph, and Hansen 1979; Doherty 1980). However, subgrain coalescence is not frequently observed.

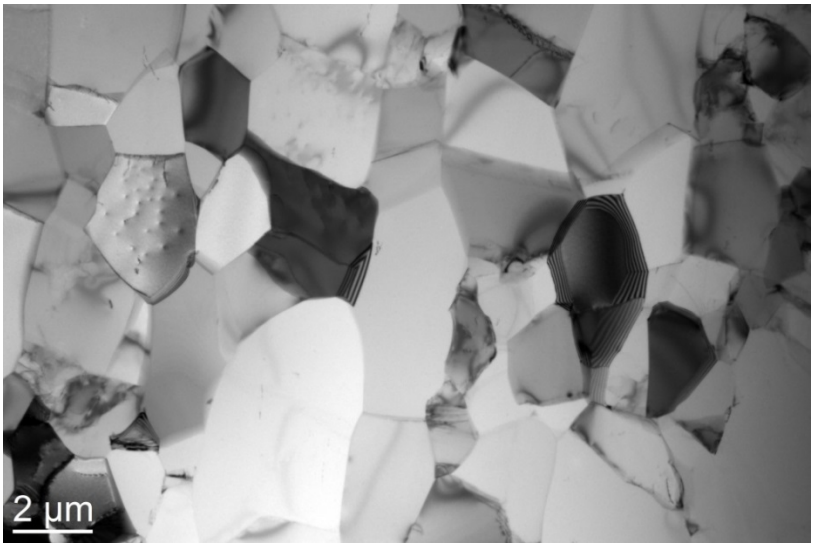

Figure 2. A well-defined subgrain structure in the longitudinal section of Al (99.9% purity) produced by 80% rolling and annealing at 255 °C for 4 h.

The kinetics of subgrain growth was commonly analyzed in analogy to grain growth, where a constant activation energy is assumed. Such an analysis neglects an important feature of recovery of a complex dislocation network structure, i.e. the increase of the activation energy during recovery (Kuhlmann 1948; Cottrell and Aytekin 1950; Borelius, Berglund, and Sjoberg 1952; Michalak and Paxton 1961; Friedel 1964; Nes 1995; Rath and Pande 2013). Consequently, many different growth exponents were reported in the literature. It should also be noted that the extent of subgrain growth is often limited due to the onset of recrystallization, thereby making it difficult for the validation of subgrain growth kinetics.

A unified coarsening model for deformation microstructures was recently proposed (Yu and Hansen 2016a). The model considers the change of the activation energy as the microstructure coarsens, and was successfully applied to

coarsening examples of different structural scales. One example is on subgrain growth as shown in Figure 3, where Q_0 is the apparent activation energy at the end of coarsening.

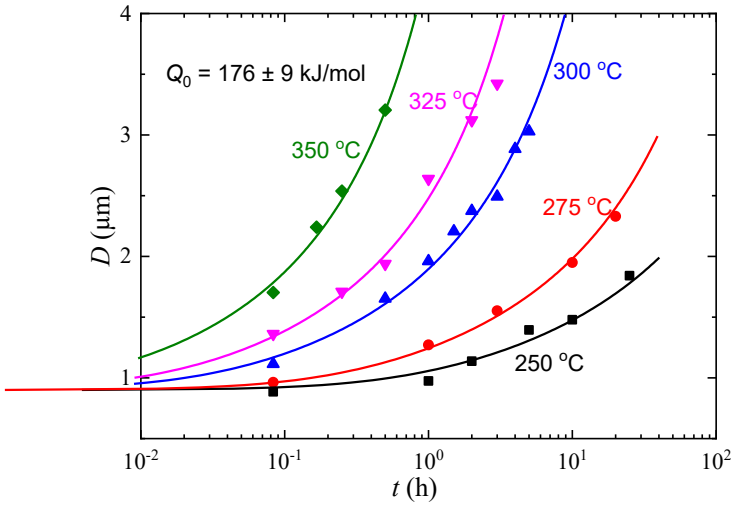

Figure 3. Isothermal subgrain growth kinetics of Al-0.05% Si single crystal channel die compressed by 70% at room temperature. The data were reported in (Y. Huang and Humphreys 2000) and later fitted by the unified coarsening model (Yu and Hansen 2016a).

2.6. Materials and processing parameters

Recovery depends on many parameters, where important ones are the stacking fault energy, solutes, second phase particles, deformation temperature, plastic strain, strain rate, and annealing temperature.

2.6.1. Material properties

A key material property is the stacking fault energy, which determines the extent to which a full dislocation dissociates into two partial dislocations, i.e. the width of the stacking fault between two partial dislocations. Therefore, in metals of high stacking fault energy such as Al and Fe, dislocations typically appear as full dislocations, which can easily climb and cross slip, and significant recovery

may take place during deformation and annealing. By contrast, in metals of low stacking fault energy such as Cu-Zn brass and Fe-Mn austenitic steel, significant thermal activation is needed for partial dislocations to constrict into full dislocations, and the recovery of the dislocation network can be slow.

The species and concentrations of solutes in the material also strongly affect recovery. Solutes may influence recovery in several ways:

- by reducing the stacking fault energy;
- by pinning dislocations;
- by pinning dislocation boundaries and thereby reducing their mobility.

Solutes retard dynamic recovery during deformation and stabilize the deformed microstructure. It leads to a higher stored energy in the deformed microstructure but also to a higher recrystallization temperature through solute drag of high angle boundaries. More significant static recovery is therefore usually observed in a solid solution than in a high purity metal. For example, there is a pronounced recovery stage in deformed arsenical Cu (Cu-0.35% As-0.05% P) but not in high purity Cu (99.98% purity) (Clareborough, Hargreaves, and West 1955).

Second phase particles in the material can also stabilize the deformation microstructure by pinning dislocations and boundaries. The drag force due to the interaction between particles and boundaries is called Zener drag, which is proportional to the volume fraction of particles and inversely proportional to the particle size.

2.6.2 Processing parameters

The deformation temperature is an important processing parameter affecting the recovery behavior. As different metals have different melting points, it is convenient to define a homologous temperature, which is the temperature divided by the melting point (T_m) in Kelvin scale. It follows that room temperature deformation may be considered as warm for Al (T/T_m=0.49) but cold for Ni (T/T_m=0.17). When a metal is deformed at a high homologous temperature, dislocations obtain a high 3D mobility and dynamic recovery occurs readily forming sharp subgrain boundaries (dynamic recrystallization may also occur if the temperature is high enough). As a result, subgrain growth becomes the main recovery mechanism for the subsequent static recovery. With decreasing deformation temperature, dynamic recovery is retarded and deformation stored energy is increased. This typically leads to pronounced static recovery during annealing, but recovery may be curtailed by an early onset of recrystallization.

The effect of strain rate is similar to that of the deformation temperature. A low strain rate provides longer time for thermal activation during dynamic recovery, thereby facilitating dynamic recovery as in the case of a high deformation temperature. As a result, the combined effect of the strain rate ($\dot{\varepsilon}$) and deformation temperature (T) can be expressed in the Zener-Hollomon parameter (Z):

$$Z = \dot{\varepsilon} \exp(\frac{Q}{RT}) \tag{3}$$

where Q is the activation energy and R is the gas constant. It should be also noted that a low Zener-Hollomon parameter not only promotes dynamic recovery but also facilities deformation, so that creep and hot deformation require a lower external stress.

With increasing plastic strain, dislocations are continuously created, accompanied by dynamic recovery. Subgrains/cells may be formed during deformation with their size decreases continuously with increasing strain. A high stored energy, as in the case of deformation at a low homologous temperature, may lead to pronounced static recovery during annealing, but may also cause early nucleation of recrystallization. In special cases where metals are only lightly deformed, the deformation microstructure may be simple and complete recovery may take place during annealing.

The annealing temperature also affects the recovery process. A high annealing temperature leads to a high recovery rate. As a number of restoration processes with different activation energy occur during annealing, a change in the annealing temperature will also change the contribution of different restoration processes, including the competition between recovery and recrystallization. A low annealing temperature usually favors recovery since many recovery mechanisms operate at a lower activation energy than that required by recrystallization (Yu, Hansen, and Huang 2012).

2.6.3 Parameter summary

In summary, dynamic recovery occurs much faster than static recovery at the same temperature due to concurrent deformation, i.e. a dynamic microstructure. The parameters affecting dynamic recovery can be analyzed by characterizing the deformation microstructure. Dynamic recovery can be enhanced by increasing the mobility of dislocations and dislocation boundaries and conditions include:

- a high stacking fault energy,
- a low concentration of solutes and particles,

- a high deformation temperature.

The rate of dynamic recovery can be also enhanced by increasing the driving force (stored energy) and conditions include:

- a high strain,
- a high strain rate.

Static recovery depends on the materials properties and the deformation microstructure. Static recovery may be enhanced by

- a high stacking fault energy
- a high stored energy
- a low concentration of solutes and particles
- a high annealing temperature

However, the last three parameters also lead to early onset of recrystallization, thereby curtailing the recovery processes. The last two parameters actually often reduce the fraction of stored energy released by recovery.

2.7 Property change during recovery

The microstructural change during recovery is accompanied by the release of stored energy and changes in physical (e.g. density and electrical resistivity) and mechanical properties (e.g. hardness and flow stress). These changes are typically smaller compared to those taking place in recrystallization.

2.7.1 Release of stored energy

The release of deformation stored energy during recovery can be measured directly by differential scanning calorimetry (DSC). However, the interpretation of the result is not straightforward since the energy release may take place by different recovery mechanisms, e.g.

- annihilation of vacancies and dislocations,
- rearrangement of dislocations into low energy configurations,
- coarsening of the cell/subgrain structure.

Moreover, precipitation and other phase transformations may also occur during annealing, and a precise relationship between the stored energy and the microstructure is difficult to establish. Instead, a simple estimation is often applied assuming all the remaining energy is stored in cell/subgrain boundaries, i.e. the stored energy (per unit volume) E_d can be expressed as

$$E_d = \alpha \gamma_s / D \tag{4}$$

where D is the cell/subgrain size, γ_S is the boundary energy, which depends on the misorientation angle, and α is a geometrical constant depending on the morphology (~3 for an equiaxed 3D structure).

The subgrain size can be readily determined by electron backscatter diffraction (EBSD) in a scanning electron microscope (SEM), and the boundary energy can be calculated based on the Read-Shockley equation, i.e. Equation (2), where the boundary misorientation angle is also determined by EBSD. However, it is often found that the stored energy estimated from this type of equations is lower than that measured directly by calorimetry.

If a cell/subgrain structure is not formed, e.g. at a very low strain, then the stored energy may be estimated as the product of dislocation density ρ and the average energy per unit length of dislocation line as

$$E_d = \frac{1}{2}\rho G b^2 \quad (5)$$

where G is the shear modulus and b is the Burgers vector. The dislocation density may be determined by measuring (i) the projected images of dislocations in a thin foil and (ii) the foil thickness in a transmission electron microscope (TEM); alternatively, it may be measured by X-ray line profile analysis (Ungár and Borbély 1996), where certain assumptions are needed in the estimation.

2.7.2 Physical and mechanical properties

The microstructural changes during recovery leads to a number of changes in the physical and mechanical properties, for example increase of density, decrease of electrical resistivity, decrease of flow stress, and increase of ductility. However, the exact relationship between these properties and the partially recovered microstructure is complex, and these properties are also affected by concurrent phase transformations. Nevertheless, recovery kinetics is commonly analyzed through measurement of the flow stress or hardness (the hardness is easier to measure and is approximately three times the flow stress). The flow stress σ is approximately related to the total dislocation density ρ (including those in cell/subgrain boundaries) as

$$\sigma = \sigma_0 + \alpha_1 M G \mathrm{b} \sqrt{\rho} \quad (6)$$

where σ_0 is the frictional stress, M is the Taylor factor, and α_1 is a constant in the order of 0.2-0.4. An example of recovery in hardness is shown in Figure 4, where cold-rolled commercial purity Al was isothermally annealed at five different temperatures and the hardness shows a quasi-logarithmic decay in the recovery range (Yu and Hansen 2016b). During annealing, the flow stress decreases with the decreasing dislocation density. However, this total dislocation density is

difficult to measure accurately. An alternative way is therefore to relate the stress to the cell/subgrain size. When the interior dislocations between cell/subgrain boundaries are ignored, the flow stress σ may be expressed in terms of the subgrain size D as

$$\sigma = \sigma_0 + kD^{-m} \quad (7)$$

where σ_0 is the frictional stress, k is a constant, and m was found to be between 0.5 and 1. Based on the flow stress σ, the extent of recovery R can be defined in terms of the flow stress of the deformed state σ_d and the flow stress of the fully recrystallized state σ_r as

$$R = \frac{\sigma_d - \sigma}{\sigma_d - \sigma_r} \quad (8)$$

Consequently, 1-R represents the residual hardening after recovery. By measuring either the stored energy E_d or the residual hardening 1-R during an annealing study, the recovery kinetics may be analyzed based on Equation (1) or other similar kinetics equations.

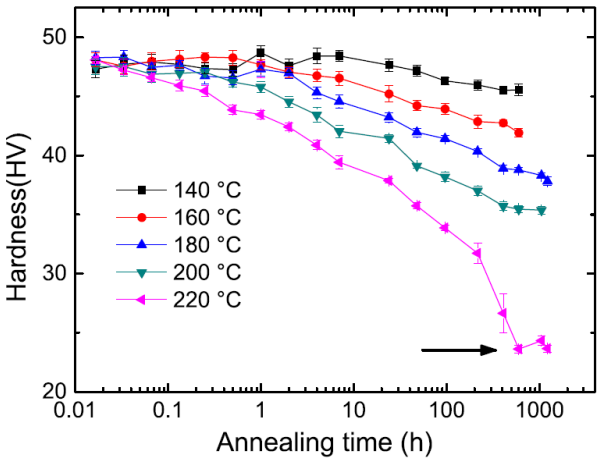

Figure 4. Hardness as a function of annealing time at the given temperatures for Al (99.5% purity) cold rolled to a true strain of 5.5. The arrow indicates recrystallized states. After (Yu and Hansen 2016b).

3. DEVELOPMENT OF DEFORMATION MICROSTRUCTURES

In the last 30 year, extensive studies (Estrin and Vinogradov 2013; Niels Hansen and Barlow 2014; Cao et al. 2018) have been carried out characterizing the detailed deformation microstructure up to an ultrahigh strain. The deformation microstructure is affected by a number of materials and processing parameters, most importantly the crystal structure, the stacking fault energy, the strain, and the deformation temperature.

For face-centered cubic (FCC) metals with highs stacking fault energies and body-centered cubic (BCC) metals, e.g. Al, Ni and Fe, deformation is typically completely accommodated by dislocation slip (Bay et al. 1992; Niels Hansen 2001; Hughes and Hansen 2004; Niels Hansen and Barlow 2014), whereas deformation twinning is negligible. Dislocations have a high 3D mobility and can easily cross slip, leading to wavy glide.

For FCC metals with low stacking fault energies, full dislocations dissociate into partial dislocations and hence cross slip becomes difficult. As a result, plastic deformation leads to a planar Taylor lattice structure (Kuhlmann-Wilsdorf 1989; Hughes 1993). With an even lower stacking fault energy, for example in Ag and many Cu alloys, deformation twinning becomes an important deformation mechanism (Wang et al. 2010; Cao et al. 2018), supplementing dislocation slip. In this case, dynamic recovery is suppressed due to the low mobility of dislocations.

For hexagonal close-packed (HCP) metals, the primary slip systems have the Burgers vectors in the basal plane. However, all of these systems put together only produce four independent slip systems and are not able to accommodate the strain along the <**c**> direction. Therefore, additional slip/twinning systems are required for a homologous plastic deformation according to the Taylor model (Taylor 1938). Such slip systems can be introduced by changing materials parameters.

Although there are some differences in the microstructural evolution of different groups of metals, the trend is similar when the strain in increased. Therefore, in the following, the microstructural evolution with strain will only be discussed for FCC metals with high stacking fault energies.

3.1 Microstructural evolution

Dislocation cells and cell boundaries have been studied for many decades but detailed microstructural characterization in the last 30 years (Bay et al. 1992; Q. Liu, Juul Jensen, and Hansen 1998; Hughes and Hansen 2000; Niels Hansen 2001; Wert, Liu, and Hansen 1997) showed that cell boundaries coexist with planar dislocation boundaries. These extended planar boundaries delineate regions that are further subdivided by cell boundaries (Figure 5). Extended boundaries

have their origin in a different range of active slip systems in neighboring regions called cell blocks. Each cell block has been assumed (Kuhlmann-Wilsdorf and Hansen 1991; Bay et al. 1992) to deform by four or fewer active slip systems, i.e. falling short of the five required for homologous deformation according to the Taylor model (Taylor 1938). However, a group of cell blocks may collectively fulfill the Taylor criterion. In such a cell block structure (Figure 5), boundaries are therefore classified into two types based on their formation mechanisms (Kuhlmann-Wilsdorf and Hansen 1991; Bay et al. 1992):

- geometrically necessary boundaries (GNBs), which are extended cell block boundaries delineating regions of different slip activities;
- incidental dislocation boundaries (IDBs), which are cell boundaries formed by mutual trapping of glide dislocations.

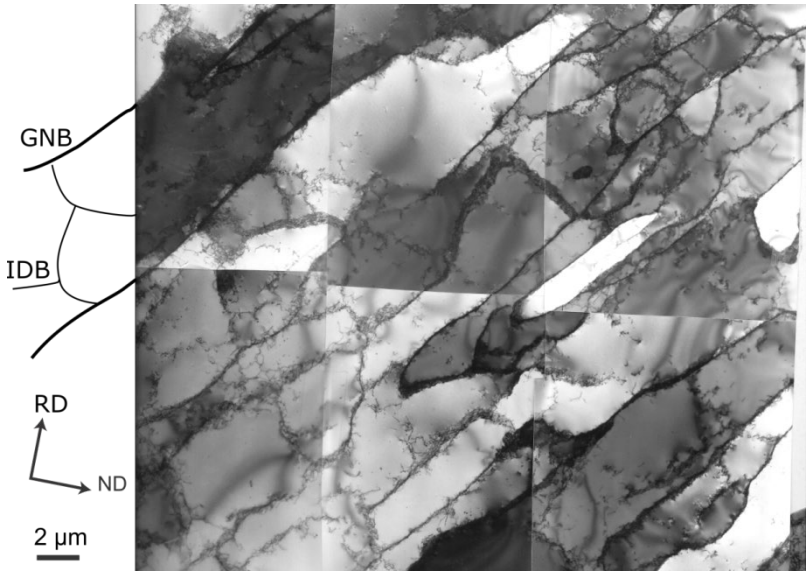

Figure 5. A cell block structure in 5% cold-rolled Al (99.99% purity) viewed in the longitudinal plane. Both GNBs and IDBs are illustrated. Courtesy of Xiaoxu Huang.

The structural morphology changes as the strain increases. After deformation to a high strain, for example by cold rolling, the structure is characterized by extended lamellar boundaries, with interconnecting boundaries and loose dislocations in the region between extended lamellar boundaries. Lamellar boundaries are categorized as GNBs and typically of medium to high angle; interconnecting boundaries are categorized as IDBs and are of low angle. An

example of such a microstructure is shown in Figure 6 for heavily cold rolled Al (Yu, Hansen, and Huang 2011). The tracing clearly shows that lamellar boundaries are not perfectly parallel or infinite. Instead, they form triple junctions, which are not in equilibrium conditions. Detailed microstructural observations (Yu, Hansen, and Huang 2011) showed that there are three types of triple junctions in the lamellar structure (Figure 7):

- Y-junctions, each formed by three lamellar boundaries;
- H-junction pairs, each formed by two lamellar boundaries and an interconnecting boundary between them;
- r-junctions, each formed by three interconnecting boundaries.

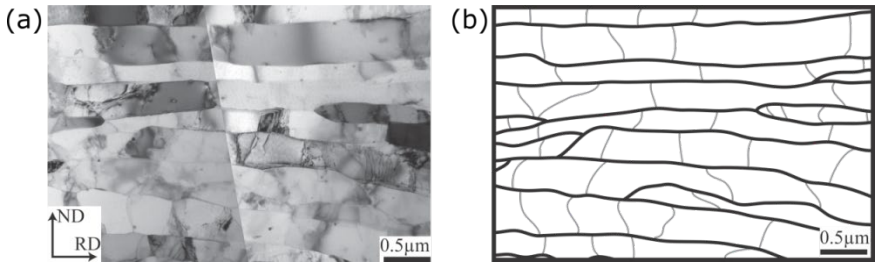

Figure 6. A lamellar structure in Al (99.5% purity) cold rolled to a true strain of 5.5. (a) TEM image viewed in the longitudinal plane; (b) tracinging of lamellar boundaries (black) and interconnection boundaries (gray). After (Yu, Hansen, and Huang 2011).

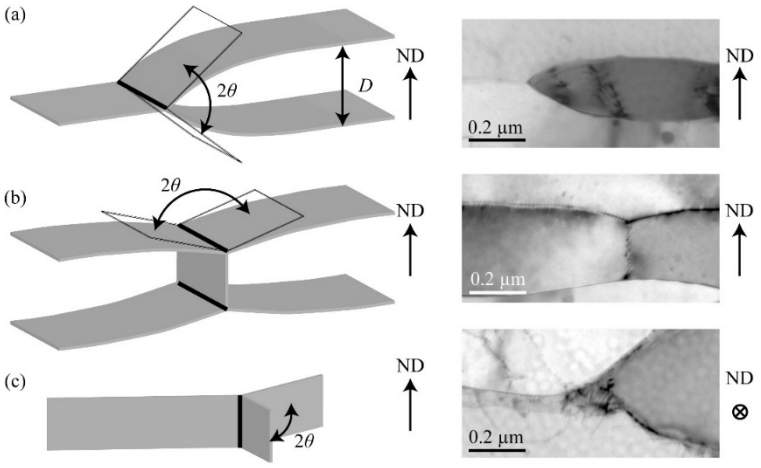

Figure 7. Illustrations and examples of three types of triple junctions in lamellar structures. (a) A Y-junction formed by three lamellar boundaries (GNBs); (b) two H-junctions (an H-junction pair) formed by two lamellar boundaries and an interconnecting boundary (IDB) between them; and (c) a r-junction formed by three interconnecting boundaries. Triple junctions are highlighted in bold lines with dihedral angles 2θ indicated. Both Y-junctions and H-junctions are lying close to the rolling plane, whereas r-junctions are oriented almost parallel to the normal direction (ND). After (Yu, Hansen, and Huang 2011).

At an ultrahigh strain, the structural refinement by deformation is counter-balanced by dynamic recovery. The structural morphology generally follows the shape change of the bulk material, for example forming a lamellar structure in rolling and a fibrous structure in wire drawing. For monotonic deformation, elongated structural morphology can be found in the longitudinal section with the aspect ratio depending on materials and processing parameters.

3.2 Microstructural parameters

Both cell block boundaries at low strains and lamellar boundaries at high strains are GNBs delineating regions with different slip activities, whereas both cell boundaries at low strains and interconnecting boundaries at high strains are IDBs formed by mutual trapping of glide dislocations (Kuhlmann-Wilsdorf and Hansen 1991; Niels Hansen 2001). For both GNBs and IDBs, the average boundary spacing decreases and the average misorientation angle across the boundary increases when the strain is increased (Figure 8). The GNB spacings and misorientation angles evolve much faster than those of the IDBs, indicating different mechanisms controlling their evolution.

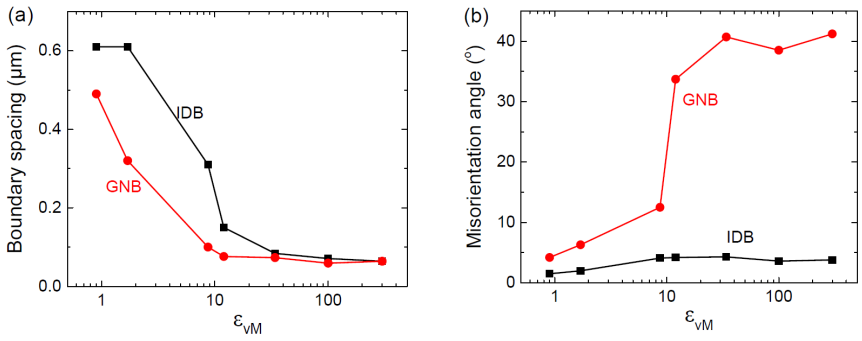

Figure 8. Boundary spacing and misorientation angle in Ni (99.5% purity) deformed by high pressure torsion (HPT) to an ultrahigh strain. (a) Boundary spacing; (b) misorientation angle. Based on data reported in (H. W. Zhang, Huang, and Hansen 2008).

When an ultrahigh strain is achieved, saturation is approached in both boundary spacing and misorientation angle. It has been showed that when Ni (99.5% purity) was deformed by high pressure torsion at room temperature, the GNB spacing reaches about 60 nm and the GNB misorientation angle reaches about 40° (H. W. Zhang, Huang, and Hansen 2008), see Figure 8. During structural refinement, there is a continuous increase in the fraction of high angle boundaries, which at large strain can approach about 60–80%. The evolution in boundary spacing is related to the dynamic recovery processes, whereas the causes behind the evolution of misorientation angle are not only dynamic recovery but also crystal symmetry and creation of new low angle boundaries.

Besides the average values of the microstructural parameters, their distributions have been studied extensively by applying a scaling hypothesis (Hughes et al. 1997; Hughes et al. 1998; Godfrey and Hughes 2000). This hypothesis is based on the assumption that similar underlying mechanisms control the formation of deformation microstructures. The scaling hypothesis reduces the amount of tasks in microstructural characterization and provides a general tool for analysis of structural parameters as demonstrated in analyses of the evolution in boundary spacing and angles with increasing strain. The distributions of these parameters at a given state depend on strain, but the scaling hypothesis demonstrates that the distributions may be represented by a strain-independent distribution using as a scaling parameter either the average boundary spacing or the average misorientation angle at each strain. The distribution functions used when applying the scaling hypothesis have been analyzed theoretically for the misorientation angle distributions (Pantleon and Hansen 2001). It should also be noted that the scaling of GNB misorientation angle breaks down at very high strains when the distribution becomes bimodal as it contains both low and high angle boundaries.

3.3 Orientation dependence

Microstructural subdivision during plastic strain can be significantly affected by the crystallographic orientation of the grain. This has been demonstrated in many single crystal and polycrystal studies (Driver, Juul Jensen, and Hansen 1994; Q. Liu and Hansen 1995; X. Huang and Winther 2007). The cause of this

orientation dependence of microstructure has been related to the orientation dependence of slip systems (Winther and Huang 2007). Three different structural types have been identified (X. Huang and Winther 2007; X. Huang and Hansen 1997) relating to the grain orientation (Figure 9):

- The type 1 structure is a cell block structure with cell block boundaries (GNBs) aligned approximately with the {111} slip planes (within 10°).
- The type 2 structure is a cell structure without GNBs.
- The type 3 structure is also a cell block structure similar to type 1, but the GNBs deviate substantially from the {111} slip planes (>10°).

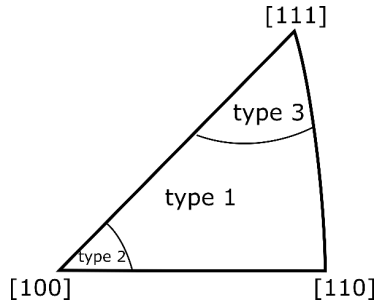

Figure 9. Crystallographic orientation of the tensile axis for three types of deformation microstructures.

The orientation dependence of microstructural subdivision leads to different stored energy depending on the local texture. In a study of deforming Al single crystals of three typical rolling texture orientations to a true strain of 1.5 (Godfrey, Hansen, and Jensen 2007), it was found that different cell block structures formed in crystals of different orientations and also showed that the stored energy is higher in {112}<111> Copper and {123}<634> S orientations than in {110}<112> Brass orientation. The difference in stored energy is expected to play an important role when the samples are annealed.

When the strain is increased during rolling, the three types of microstructures transform to a finely spaced lamellar structure, where most of the cell blocks rotate to various variants of the rolling texture components (Copper, S and Brass) separated by lamellar boundaries on a very fine scale. It was shown that rolling texture components often form wider bands than other texture components (Q. Liu et al. 2002), leading to a texture dependence of the spatial distribution of high angle boundaries. Detailed observations (Xing, Huang, and Hansen 2006) also showed that both the average GNB and IDB misorientation angles are smaller in bands of rolling texture components than in bands of other texture components.

This difference in the microstructure leads to a higher stored energy in bands of other texture components. As a result, during subsequent annealing much higher recovery rate was found in bands of other texture components (Xing, Huang, and Hansen 2006). Similar orientation dependence of deformation microstructure and recovery was reported in a study of channel die deformed Al–0.1% Mn crystals (Albou et al. 2011).

4. RECOVERY OF LAMELLAR STRUCTURES AT HIGH STRAINS

Classical analyses of recovery are largely based on the activities of dislocations and evolution of cells and subgrains. However, the deformation microstructure after a high monotonic strain (e.g. by rolling or compression) is commonly characterized by a finely spaced lamellar structure with a high fraction of high angle boundaries. The deformation stored energy is stored in these lamellar and interconnecting boundaries, and the recovery of this boundary network is important. Annihilation and rearrangement of dislocations still occur at high strain (Yu, Hansen, and Huang 2012). Due to the small boundary spacings at high strain, however, there are increased dislocation-boundary interactions and decreased dislocation-dislocation interactions.

In this section, focus is on novel recovery mechanisms in lamellar deformation microstructures. Recovery is favored in Al in the competition between recovery and recrystallization, and therefore commercial purity Al (99.5% purity) has been chosen as a model material to demonstrate important recovery mechanisms.

4.1 Microstructural coarsening during deformation

4.1.1 Removal of lamellar boundaries

The decrease of the lamellar boundary spacing with increasing strain was found to be much slower than the externally imposed shape change at large strains (Langford and Cohen 1969; Godfrey and Hughes 2000), see the sketch (Figure 10). It follows that there much be a dynamic recovery mechanism removing lamellar boundaries during deformation, counteracting the structural refinement. Such a mechanism has been recently observed experimentally during cold rolling of commercial purity Al (Yu et al. 2014).

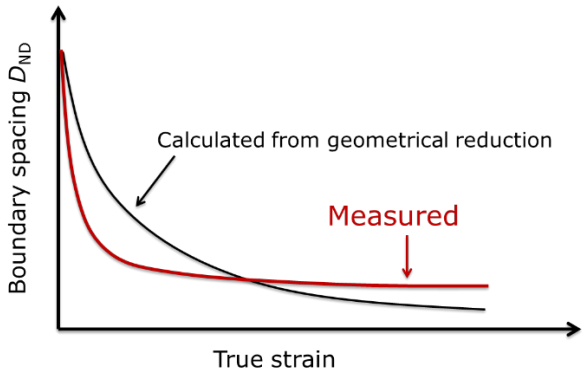

Figure 10. Illustration of the evolution of the boundary spacing measured along the ND. At low strains, the spacing decreases faster than geometrical reduction but at high strains it is slower.

4.1.2 Dynamic Y-junction migration

As shown in Figure 7a, a Y-junction is a special type of triple junctions connecting three lamellar boundaries. Consequently in a 3D structure, all lamellae are bounded by Y-junctions. In a longitudinal viewing plane, all lamellae are terminated at two Y-junctions as shown in the orientation maps (Figure 11) obtained from electron backscatter diffraction (EBSD) experiments, and the density of Y-junctions can be related to the average lamella length and spacing (Yu, Hansen, and Huang 2011). It can be further seen from Figure 11 that there are many pairs of separated lamellae with similar orientations (similar color in the EBSD orientation map). These configurations are considered as a result of break-up of lamellae followed by Y-junction migration in the bulk interior during deformation (Yu et al. 2014).

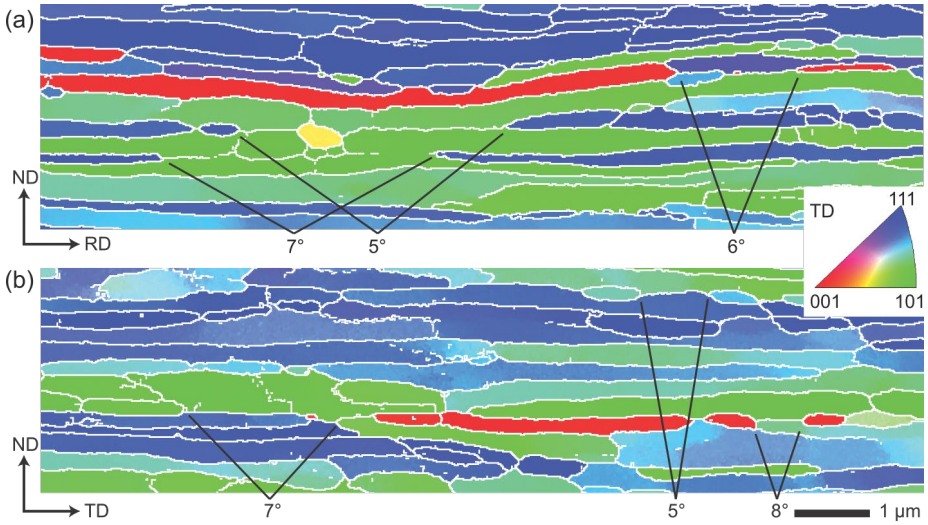

Figure 11. EBSD orientation maps showing deformation microstructures in an Al (99.5% purity) sample cold rolled to a true strain of 5.5. The maps are colored according to the crystallographic orientation of the transverse direction (TD). Separated pairs of lamellae are marked. (a) In the longitudinal section; (b) in the transverse section. After (Yu et al. 2014).

Direct evidence of Y-junction migration has also been observed during an ex situ study (Yu et al. 2014). In that study, heavily cold rolled Al was initially characterized by EBSD and electron channeling contrast (ECC) imaging in a scanning electron microscope, and then the samples were additionally cold rolled by a small amount of reduction and characterized by EBSD and ECC again. These processes were repeated a few times to follow the microstructural change in the longitudinal/transverse section during further deformation of the lamellar structure. Figure 12a shows the evolution of the microstructure in a selected area in the longitudinal section before and after additional rolling with thickness reductions of 5% and 20%. The Y-junction indicated by red arrows migrated along the RD during additional rolling, leading to a decrease of the length of the middle lamella (indicated by black arrows) and an increase of the thickness of the original neighboring lamellae. After 5% additional rolling, parts of two boundaries of misorientation angle ~20° were replaced by a single boundary of misorientation angle 4°. Figure 12b shows another example of Y-junction migration (red arrow) and also an example of break-up of a lamella (yellow arrow). The break-up of the lamella may be caused by localized shear so that two

neighboring lamellar boundaries meet each other. This creates a pair of triple junctions, and is typically followed by migration of the triple junction pair away from each other as can be seen in Figure 11.

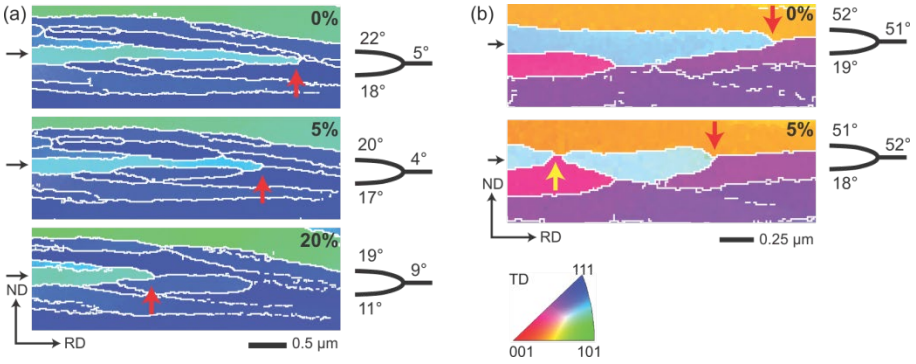

Figure 12. EBSD orientation maps showing Y-junction migration observed in the longitudinal section of cold rolled Al (99.5% purity) samples during additional cold rolling. The amounts of additional rolling are indicated within the maps. The two migrating Y-junctions are marked by red arrows, and the corresponding shortening lamellae are marked by black arrows. Boundaries with misorientation angles larger than 2° are shown by white lines, and the misorientation angles of lamellar boundaries forming the migrating Y-junctions are indicated in the sketches. (a) Initial strain 5.5; (b) initial strain 4, where the yellow arrow indicates break-up of the lamella by local shear during deformation. After (Yu et al. 2014).

Dynamic Y-junction migration counteracting the structural refinement during deformation:

- it replaces two lamellar boundaries by one, increasing the lamellar boundary spacing;
- it removes interconnecting boundaries and dislocations in swept regions, reducing the dislocation density;
- it may create low angle boundaries due to a texture effect (Figure 12a), reducing the fraction of high angle boundaries.

Dynamic Y-junction migration modifies the microstructure in a continuous manner and its directional feature leads to the retaining of the lamellar morphology. Dynamic Y-junction migration can be enhanced by thermal activation and is stress/strain assisted. Examination of large areas in heavily deformed Al revealed that this mechanism preferentially removes thin lamellae

and strongly cancels out the microstructural refinement by rolling. It rationalizes many typical features of high strain deformation, for example:

- the average lamellar boundary spacing is reduced but only to a small extent;
- the average length of lamellae decreases;
- the fraction of high angle boundaries reaches 60% ~ 80%;
- the work hardening rate is low.

The configurations shown in Figure 11 are common in deformed lamellar structures, and dynamic Y-junction migration has been observed, e.g. in tantalum deformed by high pressure torsion (Renk, Ghosh, and Pippan 2017) and Ni deformed by accumulative roll bonding (F. Liu et al. 2018).

At ultrahigh strains, the lamellar structure often has a tendency to gradually reduce its aspect ratio and become more equiaxed, due to either inhomogeneous shear deformation or enhanced boundary mobility. In this case, dynamic boundary migration loses the directional feature and becomes normal boundary migration (Legros, Gianola, and Hemker 2008; Renk et al. 2014).

4.2 Microstructural coarsening during annealing

4.2.1 Microstructural changes

The heavily deformed microstructure contains a high stored energy, serving as the driving force for recovery and recrystallization during annealing. Such a deformation microstructure can be seen in Figure 13a, showing a typical lamellar morphology (Yu, Hansen, and Huang 2013). After annealing below the recrystallization temperature, dislocation annihilation and microstructural coarsening occurred. As shown in Figure 13b, there is an increase in the lamellar boundary spacing and a decrease in the dislocation density, but the lamellar morphology was largely maintained. An important recovery mechanism has been identified accounting for this pattern of microstructural change (Yu, Hansen, and Huang 2011).

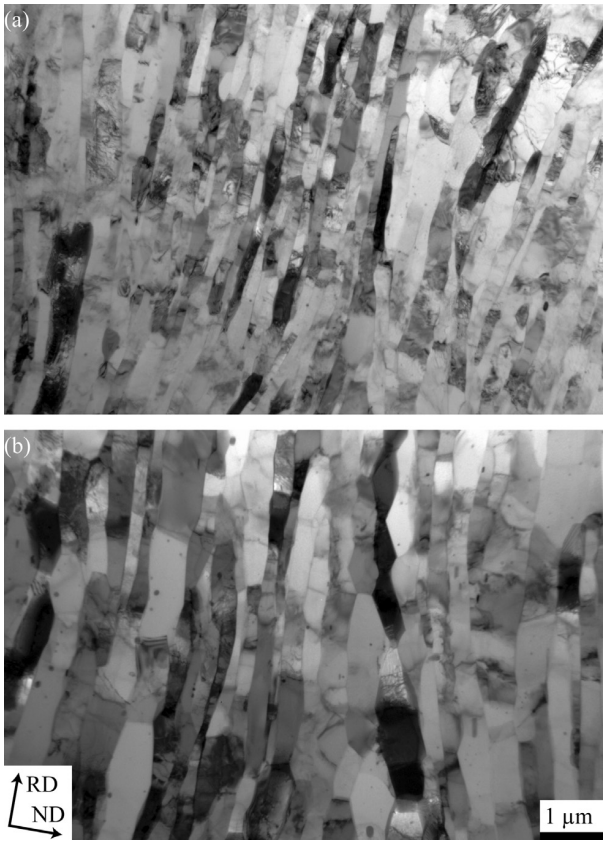

Figure 13. TEM micrographs showing microstructures in the longitudinal section of Al (99.5% purity) samples. (a) Deformed to a true strain of 5.5; (b) after annealing at 180 °C for 1 h. After (Yu, Hansen, and Huang 2013).

4.2.2 Uniform coarsening by Y-junction migration

Direct in situ and ex situ TEM observations of thin foils during annealing revealed that the uniform microstructural coarsening is due to thermally activated Y-junction migration. One example is shown in Figure 14, where a Y-junction terminating the middle lamella migrated up during annealing, leading to local increase of the lamellar boundary spacing but maintaining the lamellar morphology.

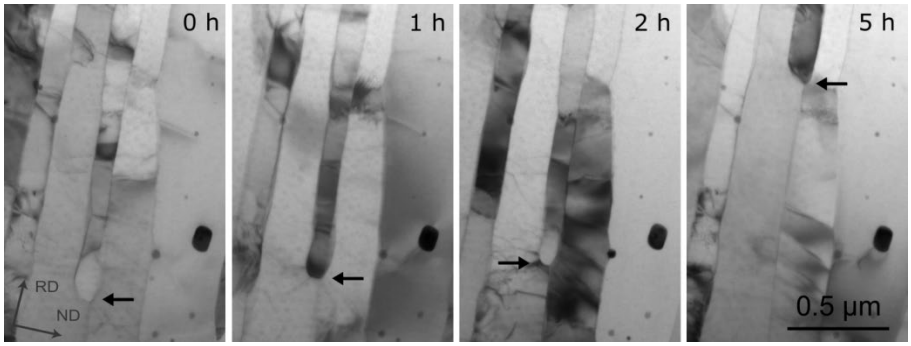

Figure 14. An example of triple junction migration observed in the longitudinal section of Al (99.5% purity) cold rolled to a true strain of 5.5 and annealed at 120 °C for different time intervals, as marked.

During migration of a Y-junction, there is a strong interaction between attached interconnecting boundaries (i.e. IDBs) and the Y-junction. Figure 15 shows such an example (Yu et al. 2015). The Y-junction in the center of the micrograph (arrowed in Figure 15a) was initially pinned by a neighboring interconnecting dislocation boundary, which was attached to one of the receding lamellar boundaries on the left side of the Y-junction. As the Y-junction migrated downwards (Figure 15b), this interconnecting boundary was forced to extend and bow, exerting a large pinning force on the connected lamellar boundary. Four dislocations are visible in this interconnecting boundary, which is sketched in Figure 15j. With further annealing, these four dislocations were unpinned successively from the moving Y-junction (Figure 15b-i). For de-pinning of each dislocation, the incubation time is much longer than the time used for glide. After all of the four dislocations in the interconnecting boundary had been unpinned, the Y-junction migrated further before it stopped near the next set of interconnecting boundaries.

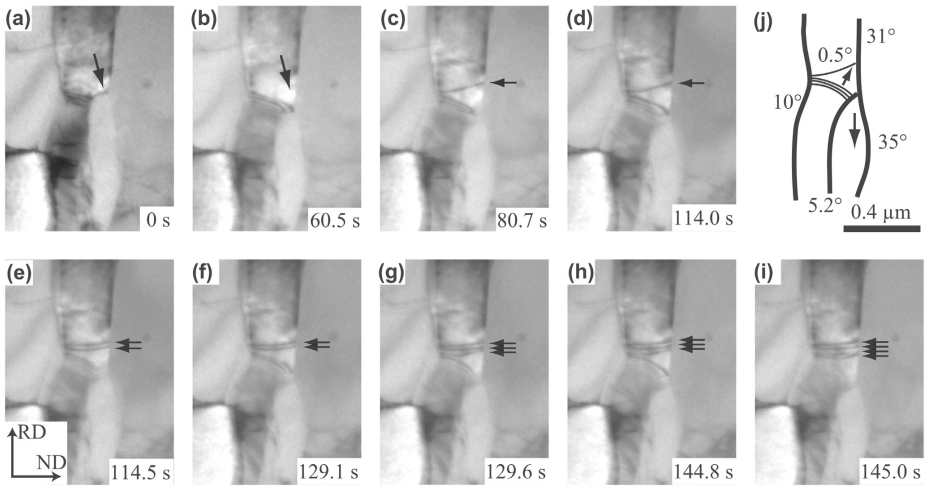

Figure 15. Migration of a Y-junction and its lengthy interaction with an attached interconnecting boundary in Al (99.5% purity) cold rolled to a true strain of 4 during annealing at 180 °C. The time sequence from 0 to 145.0 s is shown in each micrograph. The arrows in (a) and (b) point to the Y-junction, whose migration was retarded by the attached interconnecting boundary; each small arrow in (c)–(i) points to an interconnecting boundary dislocation which was unpinned after bowing. In the corresponding sketch in (j), lamellar boundaries are shown in bold lines, and the interconnecting boundary is composed of four dislocations, which are shown by thin lines. In the sketch, the big arrow indicates the direction of Y-junction migration, whereas the small arrow indicates the direction of dislocation glide during de-pinning. After (Yu et al. 2015).

Thermally activated Y-junction migration was found to be the key recovery mechanism in heavily deformed Al (Yu, Hansen, and Huang 2011; Yu, Hansen, and Huang 2013), leading to

- an increase of the lamellar boundary spacing,
- a decrease of the stored energy,
- a gradual transition from a lamellar to an equiaxed structure .

Uniform coarsening by Y-junction migration is followed by nucleation of recrystallization and growth of nuclei, and therefore it is considered as a recovery mechanism (a high strain counterpart of subgrain growth). This new recovery mechanism involves migration of deformation induced high angle boundaries and is therefore different from recovery taking place in lightly deformed microstructures.

The geometry of a Y-junction is important in determining its stability, in particular the spacing D and the dihedral angle 2θ associated with the middle lamella (Figure 7a). Thin lamellae delineated by high angle boundaries have a high tendency to be removed by Y-junction migration due to a high driving force from the grain boundary surface energy. Consequently, thin lamellae of other texture component imbedded in rolling texture components are preferentially removed, leading to sharpening of the rolling texture when a dominant texture variant is present (Mishin et al. 2013). The preferential removal of thin lamellae results in a uniform coarsening and a more symmetric distribution of the lamellar boundary spacing, i.e. the skewness of distribution decreases slightly (Yu, Hansen, and Huang 2011).

Thermally activated Y-junction migration causes uniform coarsening of deformed lamellar structures in many systems, for example pure and impure Al (T. Huang et al. 2014; Sun, Li, and Hsu 2016), Cu-Ni alloy (Tian et al. 2013), and pure and impure Ni (Y. B. Zhang, Yu, and Mishin 2017; Yu and Hughes 2018). The progress of uniform coarsening leads to the onset of recrystallization. Solutes can increase the recrystallization temperature and thereby enlarge the window for uniform coarsening by Y-junction migration (Yu and Hughes 2018).

4.2.3 Model of coarsening kinetics

The driving force for recovery coarsening results from the stored energy in the deformed materials, mainly stored in the form of deformation induced boundaries as expressed in Equation (4). The coarsening kinetics may be analyzed by combining this equation with the recovery kinetics equation, i.e. Equation (1). Such a combination leads to (Yu and Hansen 2016a):

$$\frac{dD}{dt} = k_1 D \exp(\frac{k_2}{DT}) \tag{9}$$

where k_1 is temperature dependent and k_2 is a constant, written as

$$k_1 = K_0 \exp(-\frac{Q_0}{RT}) \tag{10}$$

$$k_2 = \frac{\alpha\beta\gamma}{R} \tag{11}$$

where D is the boundary spacing, t is the annealing time, T is the annealing temperature, R is the gas constant, γ is the boundary energy, and Q_0 is the apparent activation energy at the end of recovery. The three fitting parameters K_0, Q_0 and β are associated with active recovery mechanisms.

Equation (9) can be solved with the aid of exponential integrals (Vandermeer and Rath 1990), resulting in the following relationship (D=D_0 at t=0)

$$Ei(-\frac{k_2}{DT}) - Ei(-\frac{k_2}{D_0T}) = -k_1t \tag{12}$$

where E_i( ) is the exponential integral of the quantity inside the bracket.

Equation (12) describes the continuous coarsening of a deformation structure during isothermal annealing. To estimate the model parameters k_1 and k_2 at one annealing temperature, coarsening data, i.e. (t, D) pairs, are inserted into Equation (12) and a curve of k_1 vs k_2 is calculated for each (t, D) pair. A maximum convergence point (k_2, k_1) is then determined manually by superimposing k_1 vs k_2 curves of all annealing times at that temperature. The model thus gives a fitting of the isothermal coarsening kinetics. When such a procedure is carried out for other temperatures, different convergence points (k_2, k_1) can be obtained, but the estimated temperature independent constant k_2 may vary slightly. Therefore an important subsequent procedure is to use a single average k_2 for all temperatures to re-fit the coarsening data. Such a collective fitting can reduce the fitting error significantly, especially for estimating the activation energy Q_0 based on Equation (11). Subsequently, the apparent activation energy (Q_{app}) at any stage of coarsening can be obtained as

$$Q_{app} = Q_0 - \frac{k_2R}{D} \tag{13}$$

The above coarsening model is considered to be universal for uniform coarsening of deformation microstructures (Yu and Hansen 2016a). It can be applied to both coarse structures, e.g. subgrain growth during annealing of metals deformed to low/medium strains (Figure 3), and fine structures, e.g. grain coarsening in nanocrystalline metals produced by plastic deformation to ultrahigh strains. To ensure a satisfactory accuracy, typically three to four annealing temperatures are required, in combination with four to five annealing periods at each temperature.

4.2.4 Kinetics of Y-junction migration

The kinetics of uniform coarsening via Y-junction migration can also be analyzed based on the above model. For example, it was shown that the coarsening kinetics of heavily deformed Al follows this model (Yu and Hansen 2016a). Based on Equation (12), an average value of k_2 = 1.87×10^{-3} m·K can be obtained and the corresponding coarsening curves by collective fittings are drawn in Figure 16a, showing a good agreement with the experimental data over a time

span over four orders of magnitude. The temperature dependence of k_1 can be determined by a collective fitting according to Equation (10), and it follows that Q_0 = 214±12 kJ/mol. Based on Equation (13), the dependence of the apparent activation energy on the boundary spacing can also be calculated, for example Q_{app} = 149 kJ/mol at D_0 = 0.24 μm. The apparent activation energy increases rapidly at the beginning but slowly at later stages. By combining Equations (12) and (13), one can also derive the time dependence of the apparent activation energy during annealing at different temperatures (Figure 16b). The apparent activation energy increases approximately logarithmically with the annealing time, and at a given annealing time the apparent activation energy increases with increasing annealing temperature.

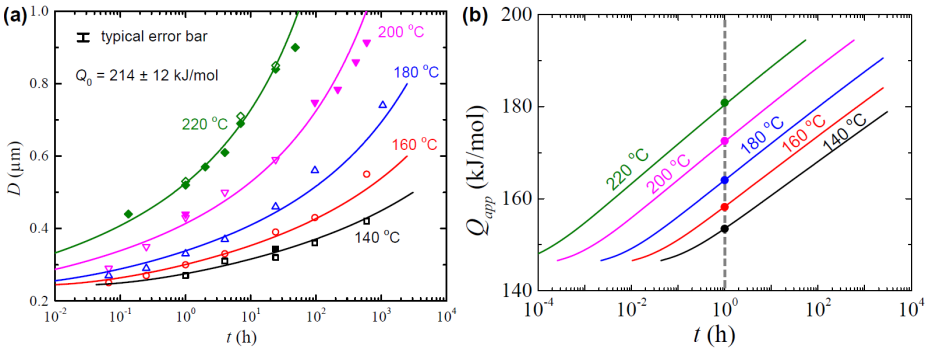

Figure 16. Recovery kinetics in Al (99.5% purity) cold rolled to a true strain of 5.5. (a) EBSD (solid symbols) and ECC (open symbols) data for the average lamellar boundary spacing during isothermal annealing at 5 different temperatures; (b) the apparent activation energy during recovery coarsening at different temperatures. After (Yu and Hansen 2016a).

The estimated apparent activation energy Q_0 is consistent with the diffusion of Fe in Al, suggesting solute drag as an important rate controlling mechanism. Lower activation energies at early stages of coarsening are related to the heavily deformed microstructure, which provides a high driving force and short-circuit diffusion paths. The model has also been successfully applied to the uniform coarsening of the deformed lamellar structure in commercial purity Ni (Yu and Hughes 2018), showing the apparent activation energy increases during annealing. The increase of the activation energy makes coarsening of deformation microstructure significantly different from grain growth in a fully recrystallized coarse microstructure, where the apparent activation energy is considered to be a constant.

4.2.5 Y-junction migration and recrystallization

Y-junction migration and recrystallization are both driven by the deformation stored energy and are competing processes during annealing. However, uniform coarsening by Y-junction migration also provides the nuclei for recrystallization. The sketch and example shown in Figure 17 indicate how Y-junction migration gradually transforms the finely spaced lamellar structure to be more equiaxed. At later stages of Y-junction migration, the activation energy was found to be similar to that for recrystallization, pointing to a continuous microstructural evolution and a strong effect of solute drag on recovery and recrystallization (Yu, Hansen, and Huang 2013).

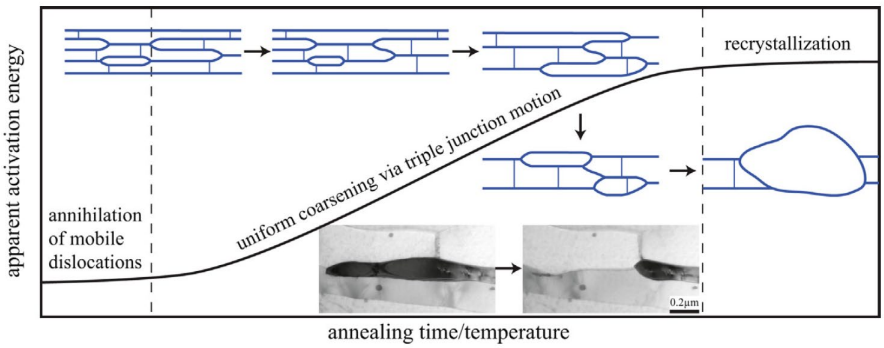

Figure 17. Sketch showing a continuous increase in the apparent activation energy and a gradual transition in the structural morphology during annealing of a deformed lamellar structure. An example of Y-junction migration is shown in the inset. After (Yu, Hansen, and Huang 2013).

5. Conclusion and Outlook

In the last 30 years, detailed microstructural characterization has led to new understandings of the deformation microstructure and recovery processes, especially for metals and alloys deformed to high strains. Quantification and analysis of structural parameters has shown for a variety of metals and processes that the microstructural evolution follows a universal and hierarchical pattern of grain subdivision on multiple length scales by the formation of GNBs and IDBs. The deformation microstructure is free of long range stresses and can be analyzed

by the low energy dislocation structure (LEDS) hypothesis. During annealing, recovery shows a quasi-logarithmic kinetics with an increasing apparent activation energy. Recovery mechanisms directly relate to the deformation microstructure, leading to a strong orientation (texture) dependence of recovery; at high strains a finely spaced lamellar deformation structure leads to uniform coarsening by Y-junction migration during deformation and annealing.

The new discoveries and understandings of deformation microstructures and recovery processes have been closely linked to the invention and development of advanced microscopic techniques, which enable structural parameters to be quantified with a high accuracy and a high speed. Novel techniques such as those based on high energy X-rays allow nondestructive characterization of bulk samples, allowing 3D in situ observations during deformation and annealing. New techniques have also been developed for chemical analysis and correlating transmission electron microscopy and atom probe tomography. An application of such techniques may lead to break-through in the understanding of the effect of solutes on recovery mechanisms and kinetics. In parallel, modelling and simulation techniques have advanced significantly and can now cover several length scales reaching towards the possibility of coupling models over multiple length scales. Further development of in situ characterization techniques provides the possibility for validation and improvement of numerical modelling, and together they are expected to bring new knowledge on deformation and annealing, so that dynamic and static recovery mechanisms and kinetics are better controlled and stronger and thermally more stable metals and alloys can be produced with less energy.

ACKNOWLEDGEMENT

This work has received funding from the European Research Council (ERC) under the European Union's Horizon 2020 research and innovation program (grant agreement No 788567). The author is grateful to Dr. Niels Hansen for his critical comments.

REFERENCES

Albou, Adeline, Andras Borbely, Claire Maurice, and Julian H. Driver. 2011. "Orientation-Dependent Recovery in Strongly Deformed Al–0.1% Mn Crystals." *Philosophical Magazine* 91 (31): 3981–4000.

Bay, B., N. Hansen, D.A. Hughes, and D. Kuhlmann-Wilsdorf. 1992. "Overview No. 96 Evolution of f.c.c. Deformation Structures in Polyslip." *Acta. Metallurgica et Materialia* 40 (2): 205–19.

Beck, Paul A. 1954. "Annealing of Cold Worked Metals." *Advances in Physics* 3 (11): 245–324.

Bever, M B. 1957. "On the Thermodynamics and Kinetics of Recovery." In *Creep and Recovery*, edited by R. Maddin, 14–51. Cleveland, OH: American Society for Metals.

Bever, M B, D L Holt, and A L Titchener. 1973. "The Stored Energy of Cold Work." *Progress in Materials Science* 17: 5–177.

Borelius, G, S Berglund, and S Sjoberg. 1952. "Measurements on the Evolution of Heat during the Recovery of Cold-Worked Metals." *Arkiv for Fysik* 6 (2): 143–49.

Cahn, R W. 1949. "Recrystallization of Single Crystals after Plastic Bending." *J. Inst. Metals* 76: 121–43.

Cao, Yang, Song Ni, Xiaozhou Liao, Min Song, and Yuntian Zhu. 2018. "Structural Evolutions of Metallic Materials Processed by Severe Plastic Deformation." *Materials Science and Engineering R: Reports* 133: 1–59.

Clareborough, L, M Hargreaves, and G West. 1955. "The Release of Energy during Annealing of Deformed Metals." *Proceedings of the Royal Society of London Series A-Mathematical and Physical Sciences* 232 (1189): 252–70.

Cottrell, A H, and V Aytekin. 1950. "The Flow of Zinc Under Constant Stress." *Journal of the Institute of Metals* 77 (5): 389–422.

Doherty, R.D. 1980. "Nucleation of Recrystallization in Single Phase and Dispersion Hardened Polycrystalline Materials." In *Proceedings of the 1st Risø International Symposium on Metallurgy and Materials Science*, edited by N. Hansen, A. R. Jones, and T. Leffers, 57–69. Roskilde, Denmark: Risø National Laboratory.

Doherty, R D, D A Hughes, F J Humphreys, J J Jonas, D. Juul Jensen, M E Kassner, W E King, T R McNelley, H J McQueen, and A D Rollett. 1997. "Current Issues in Recrystallization: A Review." *Materials Science and Engineering A* 238 (2): 219–74.

Driver, J. H., D. Juul Jensen, and N. Hansen. 1994. "Large Strain Deformation Structures in Aluminium Crystals with Rolling Texture Orientations." *Acta Metallurgica Et Materialia* 42 (9): 3105–14.

Estrin, Y., and A. Vinogradov. 2013. "Extreme Grain Refinement by Severe Plastic Deformation: A Wealth of Challenging Science." *Acta Materialia* 61 (3): 782–817.

Fæster, S, N Hansen, C Hong, X Huang, D Juul Jensen, O V Mishin, J Sun, T Yu, and Y B Zhang. 2015. *36th Risø International Symposium on Materials Science*. *IOP Conference Series: Materials Science and Engineering*. Vol. 89. Roskilde, Denmark: Technical University of Denmark.

Friedel, J. 1964. *Dislocations*. Oxford: Pergamon.

Gil Sevillano, J., P. van Houtte, and E. Aernoudt. 1980. "Large Strain Work Hardening and Textures." *Progress in Materials Science* 25 (2–4): 69–134.

Godfrey, A, N Hansen, and D J Jensen. 2007. "Microstructural-Based Measurement of Local Stored Energy Variations in Deformed Metals." *Metallurgical and Materials Transactions A-Physical Metallurgy and Materials Science* 38A (13): 2329–39.

Godfrey, A, and D A Hughes. 2000. "Scaling of the Spacing of Deformation Induced Dislocation Boundaries." *Acta Materialia* 48 (8): 1897–1905.

Hansen, Niels. 2001. "New Discoveries in Deformed Metals." *Metallurgical and Materials Transactions A* 32 (12): 2917–35.

Hansen, Niels, and Claire Barlow. 2014. "Plastic Deformation of Metals and Alloys." In *Physical Metallurgy*, edited by D E Laughlin and K Hono, 5th ed., 1681–1764. Amsterdam: Elsevier.

Huang, Tianlin, Chao Li, Guilin Wu, Tianbo Yu, Qing Liu, Niels Hansen, and Xiaoxu Huang. 2014. "Particle Stabilization of Plastic Flow in Nanostructured Al-1 %Si Alloy." *Journal of Materials Science* 49 (19): 6667–73.

Huang, X., and N. Hansen. 1997. "Grain Orientation Dependence of Microstructure in Aluminium Deformed in Tension." *Scripta Materialia* 37 (1): 1–7.

Huang, X, and G Winther. 2007. "Dislocation Structures. Part I. Grain Orientation Dependence." *Philosophical Magazine* 87: 5189–5214.

Huang, Y., and F. J. Humphreys. 2000. "Subgrain Growth and Low Angle Boundary Mobility in Aluminium Crystals of Orientation {110}<001>." *Acta Materialia* 48 (8): 2017–30.

Hughes, D. A. 1993. "Microstructural Evolution in a Non-Cell Forming Metal - Al-Mg." *Acta Metallurgica Et Materialia* 41 (5): 1421–30.

Hughes, D. A., D. Chrzan, Q. Liu, and N. Hansen. 1998. "Scaling of Misorientation Angle Distributions." *Physical Review Letters* 81 (21): 4664–67.

Hughes, D.A., and N Hansen. 2000. "Microstructure and Stength of Nickel at Large Strains." *Acta Materialia* 48: 2985–3004.

Hughes, D.A., Q. Liu, D.C. Chrzan, and N. Hansen. 1997. "Scaling of Microstructural Parameters: Misorientations of Deformation Induced Boundaries." *Acta Materialia* 45 (I): 105–12.

Hughes, D A, and N Hansen. 2004. "Plastic Deformation Structures." In *ASM Handbook*.

Hull, D., and D. J. Bacon. 2001. *Introduction to Dislocations, Fourth Edition*. Oxford: Butterworth-Heinemann.

Humphreys, F. J., Anthony D. Rollett, and Gregory S. Rohrer. 2017. *Recrystallization and Related Annealing Phenomena.* 3th ed. Amsterdam: Elsevier.

Jones, A. R., B. Ralph, and N. Hansen. 1979. "Subgrain Coalescence and the Nucleation of Recrystallization at Grain Boundaries in Aluminium." *Proceedings of the Royal Society of London Series A-Mathematical Physical and Engineering Sciences* 368 (1734): 345–57.

Kuhlmann-Wilsdorf, D. 1989. "Theory of Plastic Deformation: - Properties of Low Energy Dislocation Structures." *Materials Science and Engineering A* 113: 1–41.

Kuhlmann-Wilsdorf, D., and Niels Hansen. 1991. "Geometrically Necessary, Incidental and Subgrain Boundaries." *Scripta Metallurgica et Materiala* 25 (7): 1557–62.

Kuhlmann, Doris. 1948. "Zur Theorie Der Nachwirkungserscheinungen." *Z. Fur Phys.* 124 (7–12): 468–81.

Langford, G, and M Cohen. 1969. "Strain Hardening of Iron by Severe Plastic Deformation." *Asm Transactions Quarterly* 62 (3): 623–38.

Legros, Marc, Daniel S. Gianola, and Kevin J. Hemker. 2008. "In Situ TEM Observations of Fast Grain-Boundary Motion in Stressed Nanocrystalline Aluminum Films." *Acta Materialia* 56 (14): 3380–93.

Li, James C M. 1966. "Recovery Processes in Metals." In *Recrystallization, Grain Growth and Textures*, edited by Harold Margolin, 45–98. Metals Park, OH: American Society for Metals.

Liu, Fan, Hao Yuan, Sunkulp Goel, Ying Liu, and Jing Tao Wang. 2018. "Bulk Nanolaminated Nickel: Preparation, Microstructure, Mechanical Property, and Thermal Stability." *Metallurgical and Materials Transactions A* 49 (2): 576–94.

Liu, Q, and N Hansen. 1995. "Geometrically Necessary Boundaries and Incidental Dislocation Boundaries Formed during Cold Deformation." *Scripta Metallurgica et Materialia* 32 (8): 1289–95.

Liu, Q, X Huang, D J Lloyd, and N Hansen. 2002. “Microstructure and Strength of Commercial Purity Aluminium (AA 1200) Cold-Rolled to Large Strains.” *Acta Materialia* 50 (15): 3789–3802.

Liu, Q, Dorte Juul Jensen, and N Hansen. 1998. “Effect of Grain Orientation on Deformation Structure in Cold-Rolled Polycrystalline Aluminium.” *Acta Materialia* 46 (16): 5819–38.

Michalak, J T, and H W Paxton. 1961. “Some Recovery Characteristics of Zone-Melted Iron.” *TMS-AIME* 221 (4): 850–57.

Mishin, O.V., A Godfrey, D. Juul Jensen, and N Hansen. 2013. “Recovery and Recrystallization in Commercial Purity Aluminum Cold Rolled to an Ultrahigh Strain.” *Acta Materialia* 61 (14): 5354–64.

Nes, E. 1995. “Recovery Revisited.” *Acta Metallurgica Et Materialia* 43 (6): 2189–2207.

Pantleon, W., and N. Hansen. 2001. “Dislocation Boundaries—the Distribution Function of Disorientation Angles.” *Acta Materialia* 49 (8): 1479–93.

Perryman, E C W. 1957. “Recovery of Mechanical Properties.” In *Creep and Recovery*, edited by R. Maddin, 111–45. Cleveland, OH: American Society for Metals.

Raabe, Dierk. 2014. “Recovery and Recrystallization: Phenomena, Physics, Models, Simulation.” In *Physical Metallurgy*, edited by D E Laughlin and K Hono, 5th ed., 2291–2397. Amsterdam: Elsevier.

Rath, B.B., and C.S. Pande. 2013. “Recovery of Low-Temperature Flow Stress in Zone-Refined Aluminum Single Crystals.” *Acta Materialia* 61 (10): 3735–43.

Read, W T, and W Shockley. 1950. “Dislocation Models of Crystal Grain Boundaries.” *Physical Review* 78 (3): 275–89.

Renk, O., P. Ghosh, and R. Pippan. 2017. “Generation of Extreme Grain Aspect Ratios in Severely Deformed Tantalum at Elevated Temperatures.” *Scripta Materialia* 137: 60–63.

Renk, O, A Hohenwarter, S Wurster, and R Pippan. 2014. “Direct Evidence for Grain Boundary Motion as the Dominant Restoration Mechanism in the Steady-State Regime of Extremely Cold-Rolled Copper.” *Acta Materialia* 77 (100): 401–10.

Sandstrom, Rolf. 1977. “Subgrain Growth Occurring by Boundary Migration.” *Acta Metallurgica* 25 (8): 905–11.

Smith, C J E, and I L Dillamore. 1970. “Subgrain Growth in High-Purity Iron.” *Metal Science* 4 (1): 161–67.

Sun, Pei Ling, Wan Ju Li, and Wei Chih Hsu. 2016. “Formation of a Dominant Dillamore Orientation in a Multilayered Aluminum by Accumulative Roll Bonding.” *Journal of Materials Science* 51 (7): 3607–18.

Taylor, G I. 1938. “Plastic Strain in Metals.” *Journal of the Institute of Metals* 62: 307–24.

Tian, Hui, H L Suo, O V Mishin, Y B Zhang, D Juul Jensen, and J-C Grivel. 2013. “Annealing Behaviour of a Nanostructured Cu–45 at.% Ni Alloy.” *Journal of Materials Science* 48 (12). Springer: 4183–90.

Ungár, T., and A. Borbély. 1996. “The Effect of Dislocation Contrast on X-Ray Line Broadening: A New Approach to Line Profile Analysis.” *Applied Physics Letters* 69 (21): 3173–75.

Vandermeer, R A, and B B Rath. 1990. “Interface Migration during Recrystallization - the Role of Recovery and Stored Energy Gradients.” *Metallurgical Transactions A-Physical Metallurgy and Materials Science* 21 (5): 1143–49.

Wang, Y. B., X. Z. Liao, Y. H. Zhao, E. J. Lavernia, S. P. Ringer, Z. Horita, T. G. Langdon, and Y. T. Zhu. 2010. “The Role of Stacking Faults and Twin Boundaries in Grain Refinement of a Cu-Zn Alloy Processed by High-Pressure Torsion.” *Materials Science and Engineering A* 527 (18–19): 4959–66.

Wert, J. A., Q. Liu, and N. Hansen. 1997. “Dislocation Boundary Formation in a Cold-Rolled Cube-Oriented Al Single Crystal.” *Acta Materialia* 45 (6): 2565–76.

Winther, G., and X. Huang. 2007. “Dislocation Structures. Part II. Slip System Dependence.” *Philosophical Magazine* 87 (33): 5215–35.

Xing, Q, X Huang, and N Hansen. 2006. “Recovery of Heavily Cold-Rolled Aluminum: Effect of Local Texture.” *Metallurgical and Materials Transactions A-Physical Metallurgy and Materials Science* 37A (4): 1311–22.

Yu, Tianbo, and Niels Hansen. 2016a. “Coarsening Kinetics of Fine-Scale Microstructures in Deformed Materials.” *Acta Materialia* 120: 40–45.

———. 2016b. “Recovery Kinetics in Commercial Purity Aluminum Deformed to Ultrahigh Strain: Model and Experiment.” *Metallurgical and Materials Transactions A* 47 (8): 4189–96.

Yu, Tianbo, Niels Hansen, and Xiaoxu Huang. 2011. “Recovery by Triple Junction Motion in Aluminium Deformed to Ultrahigh Strains.” *Proceedings of the Royal Society A* 467 (2135): 3039–65.

———. 2012. “Recovery Mechanisms in Nanostructured Aluminium.” *Philosophical Magazine* 92 (33): 4056–74.

———. 2013. “Linking Recovery and Recrystallization through Triple Junction Motion in Aluminum Cold Rolled to a Large Strain.” *Acta Materialia* 61 (17): 6577–86.

Yu, Tianbo, Niels Hansen, Xiaoxu Huang, and Andy Godfrey. 2014. “Observation of a New Mechanism Balancing Hardening and Softening in Metals.” *Materials Research Letters* 2: 37–41.

Yu, Tianbo, and Darcy A Hughes. 2018. “Strong Pinning of Triple Junction Migration for Robust High Strain Nanostructures.” *Philosophical Magazine* submitted.

Yu, Tianbo, Darcy A Hughes, Niels Hansen, and Xiaoxu Huang. 2015. “In Situ Observation of Triple Junction Motion during Recovery of Heavily Deformed Aluminum.” *Acta Materialia* 86: 269–78.

Zhang, H W, X Huang, and N Hansen. 2008. “Evolution of Microstructural Parameters and Flow Stresses toward Limits in Nickel Deformed to Ultra-High Strains.” *Acta Materialia* 56 (19): 5451–65.

Zhang, Y.B., T. Yu, and O.V. Mishin. 2017. “An Electron Microscopy Study of Microstructural Evolution during In-Situ Annealing of Heavily Deformed Nickel.” *Materials Letters* 186: 102–4.